Structural Dynamics of a Catalytic Monolayer Probed by Ultrafast 2D IR Vibrational Echoes

Daniel E. Rosenfeld,* Zsolt Gengeliczki,* Brian J. Smith, T. D. P. Stack, M. D. Fayer†

Ultrafast two-dimensional infrared (2D IR) vibrational echo spectroscopy has proven broadly useful for studying molecular dynamics in solutions. Here, we extend the technique to probing the interfacial dynamics and structure of a silica surface-tethered transition metal carbonyl complex—tricarbonyl (1,10-phenanthroline)rhenium chloride—of interest as a photoreduction catalyst. We interpret the data using a theoretical framework devised to separate the roles of structural evolution and excitation transfer in inducing spectral diffusion. The structural dynamics, as reported on by a carbonyl stretch vibration of the surface-bound complex, have a characteristic time of ~150 picoseconds in the absence of solvent, decrease in duration by a factor of three upon addition of chloroform, and decrease another order of magnitude for the bulk solution. Conversely, solvent-complex interactions increase the lifetime of the probed vibration by 160% when solvent is applied to the monolayer.

Tailoring surface properties by depositing molecular monolayers (*1*) on various solid substrates is critical to many technologies, including industrial catalysis, chemical sensors (*2*), fuel cells, and molecular electronics (*3*). The functional groups terminating the monolayer determine the hydrophobicity, chemical reactivity (*4*), and charge transfer properties (*5*) of the interface, which are strongly influenced by local structure and fast associated dynamics. Despite a long-standing need, the tools to study structural dynamics of interfacial molecules under chemically relevant conditions have been lacking (*6*). Commonly used microscopy and scattering techniques provide information on the size, shape, and electronic structure of particles and adsorbates, but their time resolution is generally insufficient to study molecular dynamics, and many only function under ultrahigh vacuum conditions (*7*).

The development of ultrafast infrared (IR) spectroscopy over the past two decades has provided tools for the in-depth examination of the dynamics and structure of bulk liquids, liquids in nanoscopic environments, organic complexes, biological macromolecules, and solids (*8*–*11*). IR techniques such as pump-probe absorption, transient grating, and two-dimensional (2D) IR vibrational echo spectroscopy have been used to study spectral diffusion (*9*), vibrational relaxation (*12*), chemical exchange, (*8*, *10*), and orientational dynamics (*11*). The extension of these techniques to surfaces and interfaces has been a long-standing goal of the surface and ultrafast spectroscopy communities (*13*).

Sum-frequency generation (SFG) and second-harmonic generation (SHG) form the current basis for vibrational spectroscopy of surfaces and interfaces. Frequency-domain experiments provide important information on the molecular orientation (*14*), vibrational coupling (*15*), and hydrogen-bond network at interfaces (*16*), whereas time-domain studies can probe reorientational (*17*) and translational motions (*18*), thermal conductance (*19*), vibrational relaxation (*20*), and spectroscopic line broadening (*21*). The measurement and quantitative interpretation of 2D IR spectra of molecular adsorbates has previously been limited to thick samples and attempts at 2D IR-pump SFG-probe spectroscopy (upconverted hole-burning) (*22*, *23*). Upconverted two-pulse vibrational echoes, which measure the homogeneous component (ultrafast motionally narrowed dynamics) of the infrared absorption spectrum but cannot study spectral diffusion (time dependence of structural evolution), have been attempted as well (*21*, *24*). The frequency upconversion in time-resolved SFG renders interpretation difficult because of the included Raman process (*23*), which necessitates careful determination of the time correlation functions measured in the given beam geometry (*25*). Furthermore, SFG-based techniques are inherently insensitive because upconversion is inefficient. Techniques relying on hole-burning methods have intrinsically lower time resolution and sensitivity and produce convoluted spectra, whereas echo-based methods suffer none of these drawbacks (*26*).

Here, we report on the application of an ultrafast 2D IR vibrational echo method to molecular monolayers that overcomes all of these challenges, because there is no intrinsic tradeoff between time and frequency resolution, and the associated heterodyne detection provides much higher sensitivity (signal-to-noise ratio) than other methods. This approach opens the way for the quantitative understanding of the effect of immobilization and solvent on the structural and vibrational dynamics of molecular monolayers on solid substrates.

We applied our technique to the study of a silica-immobilized transition metal carbonyl compound of interest as a photocatalyst. Immobilized homogeneous catalysts are appealing because they maintain high molecular specificity and activity under mild conditions while precluding the need for expensive separation methods (*27*–*29*). However, conditions such as the presence or absence of solvent can strongly affect catalytic activity in presently unpredictable ways (*29*, *30*). Microscopic changes affecting molecular reactivity should manifest themselves in the dynamical characteristics of the system due to the small energy differences among states. As a first step toward resolving solvent-dependent vibrational dynamics that could ultimately assist rational catalyst optimization, we have compared spectral diffusion rates and vibrational lifetimes of bare (monolayer/air interface) versus solvated surface-bound complexes. In addition, the dynamics of the immobilized catalyst are compared to the corresponding homogeneous catalyst in bulk solution.

We immobilized a compound in the $LRe(CO)_3X$ class of complexes (L, heteroaromatic bidentate ligand; X, halide/pseudohalide) that are under investigation as homogeneous photo/electro-catalysts for the reduction of CO_2 to CO or formate (*30*). Other metal-ligand–based catalysts have been immobilized (*27*), and the system depicted in Fig. 1 represents a good model system for studying

Department of Chemistry, Stanford University, Stanford, CA 94305, USA.

*These authors contributed equally to this work.
†To whom correspondence should be addressed. E-mail: fayer@stanford.edu

immobilized catalysts in general. The planarity and optical transparency of the substrate facilitates optical study.

We prepared the molecular monolayer by tethering *fac*-RePhen(CO)$_3$Cl (Phen, phenanthroline) to an undecane monolayer through a triazole linker, created by Cu(I)-catalyzed 1,3-dipolar Huisgen cyclization between a terminal alkyne and an organoazide, popularly referred to as a "click" reaction (*27*, *31*) (Fig. 1, A to C). The undecane monolayer is attached to a 100-nm-thick silica layer grown on a calcium fluoride substrate [see Supporting Online Material (SOM) for details].

The *fac*-RePhen(CO)$_3$Cl head group has three CO stretching modes that absorb strongly in the infrared. For the monolayer/air interface (Fig. 1D), the peaks are at 1898 cm^{-1} (ν_1), 1921 cm^{-1} (ν_2), and 2022 cm^{-1} (ν_3). The ν_3 transition is a nearly symmetric stretch involving all three carbonyls. The band shifts to higher frequency and narrows when the surface is submerged in chloroform (Fig. 1E). The blue shift and peak narrowing are more pronounced in a bulk solution of the RePhen(CO)$_3$Cl head group (Fig. 1, C and F, and Table 1). We chose to study the ν_3 transition because it is well resolved spectroscopically and acts as a probe of the effects of the heterogenization and solvent on the metal complex. The absorbance [optical density (OD)] for the ν_3 transition was ~5×10^{-4} which gave a sufficient signal-to-noise ratio in the 2D IR experiments. The monolayer was monitored for degradation by frequent Fourier transform infrared (FTIR) analysis and was found to be inert and stable over the course of all experiments.

The tilt angle of the transition dipole moment for the ν_3 transition with respect to the surface normal was determined to be 63 ± 1° at the monolayer/air interface from the polarization dependence of the FTIR spectrum when the incident angle was Brewster's angle (*32*, *33*). When the monolayer was submerged in chloroform, the ν_3 transition dipole tilt shifted to 57 ± 1°, indicating only small structural changes upon solvation. By performing the same analysis for all three modes, the absolute orientation of the head group in the monolayer was determined. Four optically indistinguishable configurations of the ligands around the Rhenium atom were found (fig. S4).

We determined the coverage of the monolayer with infrared spectroscopy using the absorbance, the molecular orientation, and the extinction coefficient. These results were confirmed with inductively coupled plasma mass spectrometry (ICPMS), which measures the total rhenium content (table S2). The surface coverage was 1.9×10^{14} molecules per cm^2 (53 Å^2 per molecule), which is in line with the typical surface coverage of transition metal complexes (*34*) and indicates that we obtained a molecular submonolayer.

Details of the 2D IR vibrational echo spectroscopy method have been given elsewhere (*35*). In the experiments, three ~100-fs IR laser pulses tuned to the frequency of the ν_3 mode are crossed in the sample. The three pulses generate a nonlinear polarization that emits the vibrational echo pulse (the signal) in a unique direction; this pulse is subsequently detected as a function of frequency, ω_m (the vertical axis in the 2D spectra) by optical heterodyning, which provides phase information and amplifies the signal. The first laser pulse starts a coherent oscillation of the vibrational oscillators, effectively labeling the initial frequency of each oscillator, ω_τ (the horizontal axis in the 2D IR spectra). At a time τ later, the second laser pulse stops this coherent oscillation and starts the population period of duration T_w (the waiting time) by driving the system into vibrational population states. The third laser pulse ends the population period and triggers the emission of the vibrational echo pulse. During the second time period of length T_w, the excited vibrations can undergo frequency evolution, vibrational relaxation, or other dynamic processes. The frequency evolution (spectral diffusion) during the T_w period can be characterized by a frequency-frequency correlation function (FFCF), which is typically modeled as a sum of exponential decays.

The 2D IR spectra of the ν_3 mode were acquired for the monolayer (bare, Fig. 2A), the same monolayer under chloroform (wet, Fig. 2B), and the bulk chloroform solution of the RePhen(CO)$_3$Cl head group (Fig. 2C). The large inhomogeneous components and slow spectral dynamics of the interfacial systems are reflected in the elongated shape of the absorption peaks at T_w = 0.5 ps, and their slow changes in shape with increasing T_w. The 2D IR spectra of the bulk solution show clear differences relative to the monolayer complexes: The central peak is less elongated at short time, which indicates a larger homogeneous component, and also undergoes more substantial change in shape with increasing time, demonstrating that spectral diffusion is much faster than in the monolayer samples.

The rate of the spectral diffusion is quantified with the well-established center-line-slope (CLS) method (Fig. 3, A and C) (*36*, *37*). A clear trend is observed in the CLS decay time constant, which decreased from 78 ± 15 ps for the bare monolayer to 26 ± 4 ps for the wet interface, both substantially slower than the 5 ± 1 ps measured for the head group in bulk solution. The fast spectral diffusion time constant for the complex in bulk solution is consistent with fast structural evolution (rotation/translation) of the solvent surrounding the complex that results in fast sampling of the heterogeneous solvation microstates. This is clearly not the case when the complex is immobilized on the surface (compare CLS decays in Fig. 3, A and C).

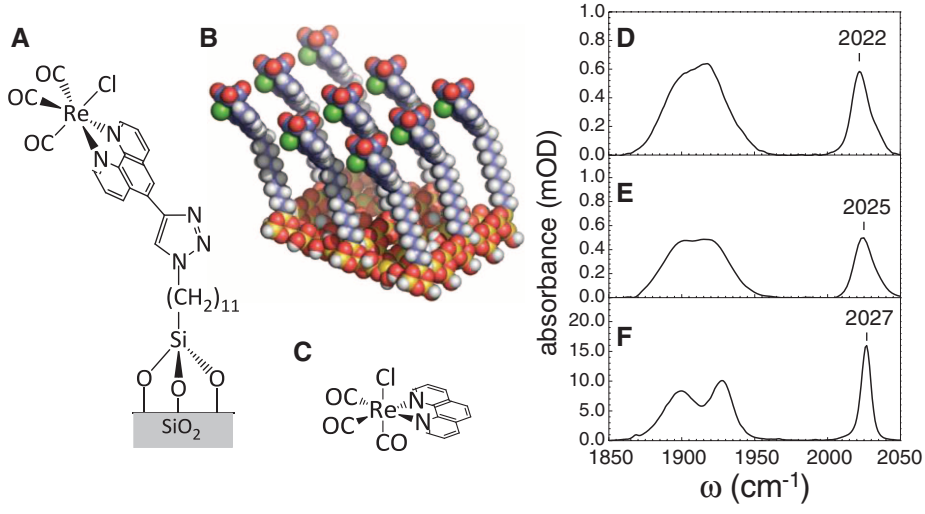

Fig. 1. (**A**) The molecular structure of the heterogenized catalyst in the monolayer. (**B**) Schematic illustration of a monolayer of the heterogenized catalyst on silica. (**C**) The structure of the *fac*-RePhen(CO)$_3$Cl molecule used in the bulk solution experiments. (**D** to **F**) Linear infrared absorption spectra of the three CO stretching modes of (D) the heterogenized catalyst monolayer/air interface, (E) the monolayer/chloroform ($CHCl_3$) interface, and (F) *fac*-RePhen(CO)$_3$Cl in bulk chloroform solution

Table 1. Dynamic and static parameters determined from experiments. Δ is the full width half maximum of the ν_3 transition, Δ_H is the homogeneous full width half maximum of the ν_3 transition, and Δ_I is the inhomogeneous full width half maximum of the ν_3 transition.

Sample	ν_3 (cm^{-1})	Δ (cm^{-1})	Δ_H (cm^{-1})	Δ_I (cm^{-1})	T_{VR} (ps)	T_{SSD} (ps)
Monolayer, bare	2022	15.2	1.8	14.3	10 ± 2	120–180
Monolayer, wet	2025	11.9	2.4	10.6	16 ± 2	40–60
Bulk solution	2027	7.9	3.5	6.5	30 ± 3	5 ± 1

The homogeneous linewidth (very fast structural fluctuations that produce motional narrowing) is associated with the difference between 1 and the value of the CLS curve at $T_w = 0$. Here, again, there is a clear trend. The homogeneous component of the FFCF increases from 12% for the bare monolayer to 20% at the wet interface, indicating substantial additional motional narrowing. For the bulk solution of the head group, the homogeneous component of the linewidth accounts for nearly 50% of the total absorption line broadening, indicating drastic differences in the solvation of the surface bound complex versus the bulk solution. The homogeneous and inhomogeneous linewidths can be recovered directly from the CLS method (*36*) and are listed in Table 1. We can conclude that the solvent has rendered some of the heterogeneous microstates of the bare monolayer spectroscopically equivalent when the monolayer is exposed to solvent.

After excitation, vibrations relax to the ground vibrational state with the lifetime, T_{VR}. Vibrational relaxation conserves energy and so requires lower frequency molecular modes, including collective modes of the surroundings (phonons), in which to deposit the energy (*38*). Vibrational relaxation time constants are highly sensitive to molecular structure, the local environment, and the phonon density of states. To measure the vibrational lifetime, we operated the 2D IR spectrometer in a heterodyne-detected transient grating (HDTG) configuration using a new approach, as outlined in the SOM. This method overcomes technical challenges associated with standard IR pump-probe experiments in measuring vibrational relaxation in samples with very low absorption.

Figure 3, B and D, shows the HDTG decays (points) and single exponential fits (curves) for the bare and wet monolayers as well as the bulk solution. The vibrational lifetime increased steadily from the bare monolayer to the wet monolayer to the bulk solution (Table 1). The vibrational lifetime might rather be expected to decrease upon addition of solvent as the phonon density of states increases. Therefore, the observed lifetime increases are likely due to changes in the anharmonic coupling of the ν_3 mode to intramolecular acceptor modes.

Both the frequency and the vibrational lifetime of a metal carbonyl vibration are inversely correlated with the amount of π back-bonding from the metal into π* antibonding molecular orbitals of the CO ligands (*15*). The ν_3 vibration shifts to higher frequency and relaxes more slowly when the monolayer is in contact with the chloroform liquid. The lifetime increases further and the frequency shifts further blue when the complex is fully immersed in bulk chloroform. These changes are consistent with diminished π back-bonding in the $Re(CO)_3$ moiety on exposure to chloroform (*15*).

The changes in π back-bonding are consistent with a CH-π interaction between the chloroform and the phenanthroline ligand, which will affect the electron density of the metal CO system (*39*). The electron density of the phenanthroline will be inductively drawn away from the Re, which will decrease the amount of π back-bonding. The same π back-bonding changes that affect the ν_3 spectra and vibrational lifetimes could influence the catalytic activity of the immobilized metal complex because increases in π back-bonding decrease the CO bond order but augment the strength of the Re-C bond (*39*).

The 2D IR data show that the solvent significantly increases the rate of spectral diffusion and, as will be discussed below, the rate of structural evolution. However, even in the absence of solvent, there is substantial spectral diffusion. In samples with nearly full monolayer coverage, vibrational excitation transfer (Förster transfer) between molecules that are close to each other but have different frequencies can be a source of spectral diffusion (*40*). Therefore, both structural spectral diffusion (SSD) and excitation transfer–induced spectral diffusion (ETISD) can contribute to the measured spectral diffusion. Both SSD and ETISD processes can be affected by the addition of solvent. The solvent can affect microscopic structural fluctuations that are responsible for SSD and change the homogeneous and inhomogeneous contributions to the vibrational line shape, which independently will affect ETISD. To separate the contributions of structural evolution and excitation transfer to the measured spectral diffusion, a new excitation transport theory has been developed. Vibrational excitation transport depends on the spatial separation between molecules, the relative orientations of the vibrational transition dipoles, the homogeneous and inhomogeneous contributions to the vibrational line shapes, and the vibrational lifetime. We measured all of these necessary parameters.

Two vibrational chromophores in spatial proximity that have significant spectral overlap of their homogeneous lines will undergo ET via the Förster mechanism at a significant rate (*41*). ET processes are extremely sensitive to geometry and spatial proximity due to their r^{-6} distance dependence. That the exchange depends on the overlap of the homogeneous lines of the vibrations on two molecules is an important caveat. The overlap of the vibrational homogenous linewidths of two molecules that have different center frequencies enables conservation of energy in the excitation transfer process. Two vibrational oscillators that are close together spatially and close in frequency will undergo fast exchange, whereas two oscillators that have the same spatial separation but that are farther apart in frequency will undergo much slower exchange. Figure 4A shows the Gaussian absorption line and the underlying homogeneous Lorentzians. The slow excitation transfer for vibrations that are far apart in frequency is caused by small overlap of their homogeneous lines, which results in a small Förster radius. The inset shows calculations of the temporal decay of the probability that the initially excited molecule

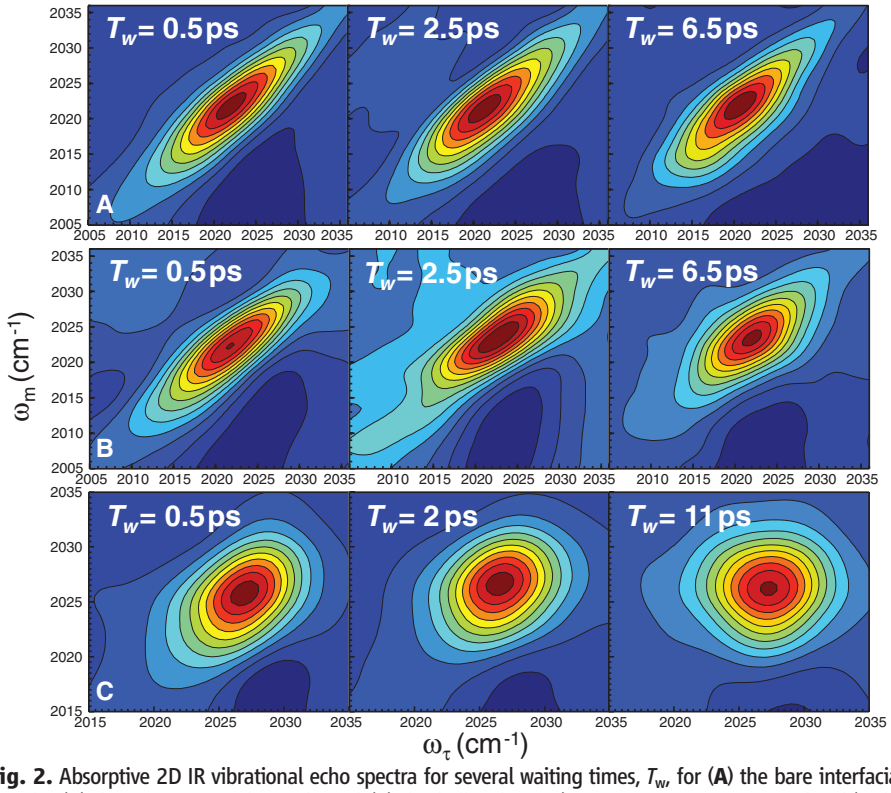

Fig. 2. Absorptive 2D IR vibrational echo spectra for several waiting times, T_w, for (**A**) the bare interfacial sample, (**B**) the wet interfacial sample and (**C**) the bulk solution (see Section IV of SOM for details). The rate of spectral diffusion increases upon addition of solvent.

remains excited [$P_{in}(t)$] for transfer between the red spectra and between the blue spectra in the main part of the figure. In this calculation, the molecules are 8 Å apart.

The 2D IR experiments (Figs. 2 and 3 and Table 1) provide the homogeneous linewidths, without which the ET calculations would be impossible. In addition, it is necessary to know the transition dipole (0.27 D), which was determined from the absorption spectrum, the vibrational lifetime (Fig. 3, B and D, and Table 1) to determine the quantum yield, and the direction of the transition dipole, which was measured with polarized FTIR. Finally, it is also necessary to know the surface coverage, which was determined both by FTIR absorption and ICPMS. The surface coverage sets the distance scale for the ET.

The ETISD can be calculated by solving the excitation transfer problem for a given geometry and distribution of frequencies (see SOM). We examined three possible geometries conforming to the measured surface coverage: hexagonal close-packed (HCP), a loose random circle packing (LP) that has a hard disk radial distribution function, and a uniform random distribution with excluded area (RE). We are able to exclude HCP and LP based on the fact that the ETISD-only FFCF decays faster than the experimentally observed decay (see SOM). Only the RE structure is physically consistent with the experimental data. In Fig. 4B, we show the experimentally determined exponential decay of the FFCF with T_w for the bare sample (circles) and its fit (black curve), as well as two calculated curves for the RE structure. The solid curve is a complete numerical solution to the transfer problem, and the dashed curve uses the Huber cumulant expansion approximation (*42*), which is seen to be quite accurate.

The exclusion radius in the RE model defines the excluded area that prevents the initially excited molecule from physically overlapping with a nearby acceptor molecule. Based on the size of the complexes, it is possible to bound the exclusion radius between 6.25 Å and 7.5 Å (fig. S10). In Fig. 4B, the exclusion radius is chosen to be 6.5 Å (a molecular radius of about 3.25 Å), which is consistent with the calculated van der Waals radius of the Rhenium complex.

The total spectral diffusion, which is measured experimentally, can be separated into the SSD and ETISD components using a theory that accounts for both types of spectral diffusion. In connection with Fig. 4A, we saw that the rate of excitation transfer depends on the frequency separation of the chromophores in addition to their spatial separation. Structural evolution of the system causes the frequencies of the vibrations to evolve in time, which is the source of SSD. SSD can bring two frequencies close together or can move them farther apart, resulting in a greater or lower probability of ET, respectively. Therefore, in addition to the time-independent spatial distribution of chromophores, the time-dependent SSD must be included in the ET calculation. We have developed the theoretical methodology to accomplish the calculation of combined SSD and ETISD using the Huber cumulant expansion (*42*), which we have shown to be accurate for describing the excitation transfer in this system (see Fig. 4B and SOM). Figure 4C illustrates the theoretical methodology that we implement. Frequency trajectories from the simulated SSD stochastic process are drawn for each oscillator, and the excitation transfer problem is propagated at each time step using the instantaneous frequencies of each oscillator and the Huber cumulant approximation.

Figure 4D shows the experimental FFCF for the bare monolayer (circles) and ETISD curves with the exclusion radius between 6.25 and 7.5 Å (shaded region). For the calculated total spectral diffusion to match the experimental data, the structural spectral diffusion time constant must fall between 120 ps and 180 ps as hard limits. The red and blue solid curves through the data correspond to these bounds, which come from the red and blue dashed curves that are the limits of the shaded region. Figure 4E shows the same information for the wet monolayer. Because the wet sample is the same monolayer/substrate as the bare sample except that it has been immersed in the solvent, the spatial distribution is the same. However, the wet monolayer ETISD calculations include the changes in the homogeneous and inhomogeneous linewidths in going from bare to wet (Table 1). To match the total spectral diffusion with the experimental data, the SSD time constant must fall between 40 ps and 60 ps as hard limits.

The structural spectral diffusion time constants, which can only be measured from 2D IR spectroscopy, quantify the structural dynamics of the interfacial layer because the structural motions of the monolayer and surrounding molecules are coupled to the vibrational frequency. One mechanism of SSD that has been demonstrated for the CO stretching mode of CO bound to Fe-heme in the protein myoglobin (*43*) and for the hydroxyl stretch of water (*44*) is the Stark effect. Motions of molecules bound to the surface can produce fluctuating electric fields that cause spectral diffusion. Therefore, the spectral diffusion of the bare sample is reporting on the time scale of motions of the surface-attached molecules. The results show that even the bare layer has relatively fast structural motions, ~150 ps. The relatively short time scale associated with the bare surface structural dynamics shows that the immobilized Re complex is far from static even in the absence of a solvent.

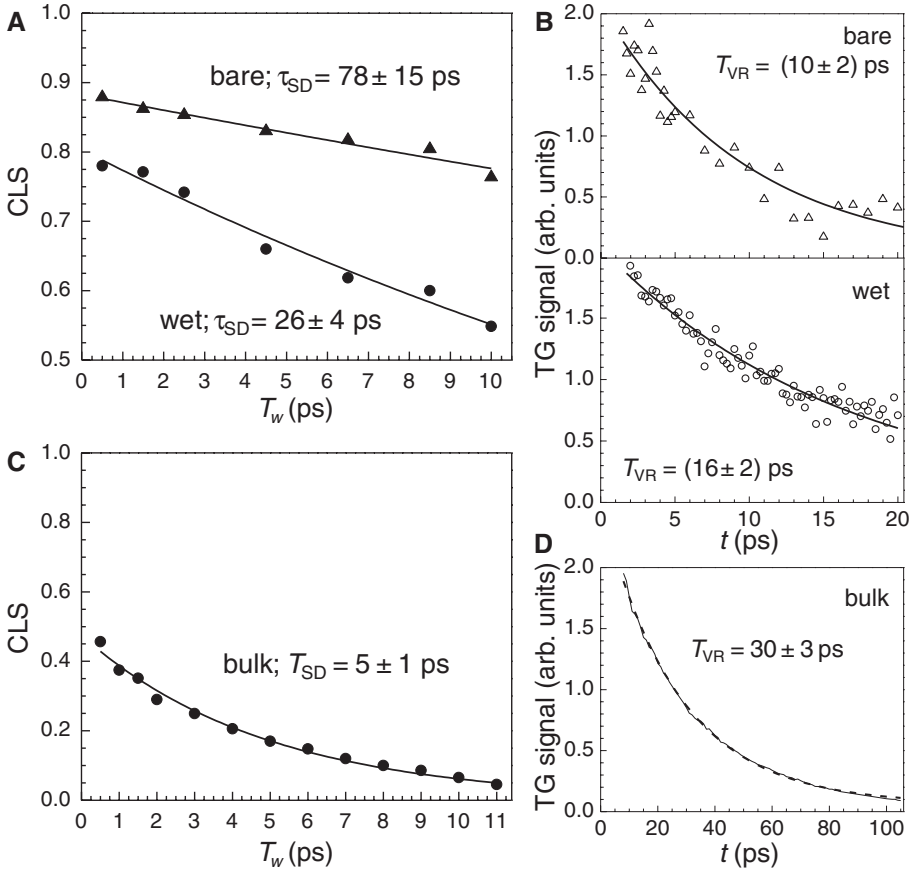

Fig. 3. Vibrational dynamics data and fits. (**A**) The CLS decay data for the bare and wet monolayers. (**B**) The transient grating lifetime decay for the bare and wet monolayers. (**C**) The CLS decay data for the bulk solution. (**D**) Transient grating lifetime decay of the *fac*-RePhen(CO)$_3$Cl complex in solution (solid = data, dashed = fit). The addition of solvent accelerates spectral diffusion and the vibrational relaxation.

Addition of the $CHCl_3$ solvent changes the time scale of structural fluctuations from ~150 ps to ~50 ps. This time should be compared to the spectral diffusion time constant of 5 ps for the *fac*-RePhen$(CO)_3$Cl head group in bulk $CHCl_3$ solution. Therefore, the functionalized surface molecules in contact with the solvent have motions that are very different from those of a fully solvated metal complex. The increase in the rate of spectral diffusion for the wet surface sample is unlikely to be due strictly to solvent dynamics. The bulk solution sample has a very large homogeneous width (Fig. 3 CLS data and Table 1), 3.5 cm^{-1} compared to an inhomogeneous width of 6.5 cm^{-1}. In contrast, the wet surface sample has a homogeneous width of 2.4 cm^{-1} compared to an inhomogeneous width of 10.6 cm^{-1}. Furthermore, the wet sample vibrational lifetime is 60% shorter than the bare sample, but the bulk solution sample's lifetime is 300% slower than the bare sample. The stark contrast between the solvated monolayer and the solvated bulk complex demonstrate that the solvent changes the structural dynamics of the metal complexes in the monolayer in a different manner than in the bulk. If the addition of solvent to the monolayer simply added structural fluctuations of the solvent to the SSD of the monolayer, one would expect to see a ~5-ps component, which is not present. The solvent might disentangle the carbon chains, resulting in the small observed change in head group angle and facilitating faster molecular motions. Experimental and molecular dynamics simulation studies of the dependence of the rate of spectral diffusion on the chemical nature of the solvent will help determine the role the solvent plays in the dynamics of this and other functionalized surfaces (*43*).

Using ultrafast 2D IR vibrational echo spectroscopy, HTDG experiments, and FTIR studies, we have examined the dynamics and structure of a monolayer of molecules bound to a planar SiO_2 surface. The experiments open up a long-anticipated field. Our general methodology when systematically applied across solvents, monolayer coverage, and metal complexes or other vibrational dynamics labels can provide greatly increased understanding of the structural and vibrational dynamics of molecules on surfaces and at interfaces.

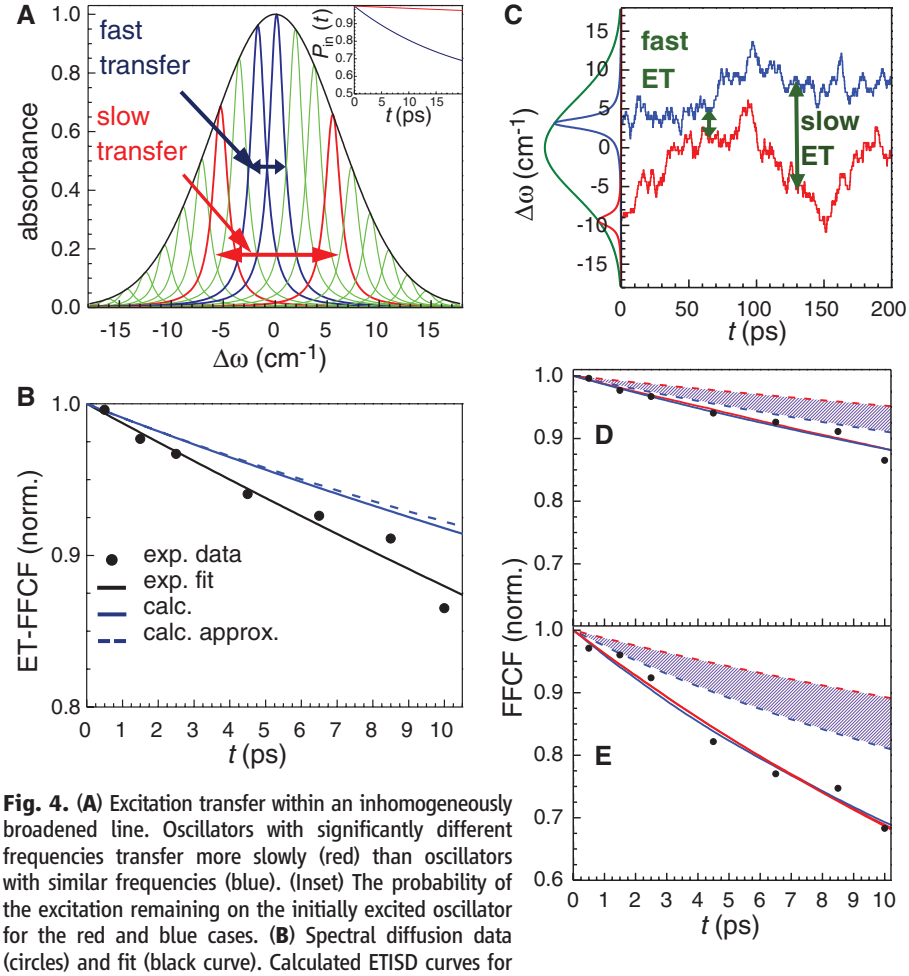

Fig. 4. (**A**) Excitation transfer within an inhomogeneously broadened line. Oscillators with significantly different frequencies transfer more slowly (red) than oscillators with similar frequencies (blue). (Inset) The probability of the excitation remaining on the initially excited oscillator for the red and blue cases. (**B**) Spectral diffusion data (circles) and fit (black curve). Calculated ETISD curves for the random distribution with excluded area effect model (solid blue line, exact numerical solution; dashed blue line, approximation). (**C**) Illustration of the influence of spectral diffusion on excitation transfer. Two frequency trajectories are drawn from the inhomogeneous distribution (green Gaussian), and excitation transfer can occur at each time step. The transfer is faster when the frequencies approach each other and slower when they are apart. (**D**) Total spectral diffusion (SSD and ETISD) for the bare monolayer (points, experimental data; black curve, fit). The shaded region is the set of possible ETISD curves. The blue and red lines show the normalized FFCF after inclusion of a 180-ps SSD decay and a 120-ps SSD, respectively, which are based on the dashed red and blue lines that bound the possible ETISD decays. (**E**) Total spectral diffusion (SSD and ETISD) for the wet monolayer. Blue and red lines denote 60- and 40-ps SSD decays, respectively, which are based on the dashed blue and red lines that bound the possible ETISD decays.

References and Notes

1. J. J. Gooding, S. Ciampi, *Chem. Soc. Rev.* **40**, 2704 (2011).
2. J. J. Gooding, F. Mearns, W. Yang, J. Liu, *Electroanalysis* **15**, 81 (2003).
3. J. S. Lindsey, D. F. Bocian, *Acc. Chem. Res.* **44**, 638 (2011).
4. S. F. Bent, J. S. Kachian, J. C. F. Rodríguez-Reyes, A. V. Teplyakov, *Proc. Natl. Acad. Sci. U.S.A.* **108**, 956 (2011).
5. D. M. Adams *et al.*, *J. Phys. Chem. B* **107**, 6668 (2003).
6. G. A. Somorjai, Y. Li, *Proc. Natl. Acad. Sci. U.S.A.* **108**, 917 (2011).
7. G. A. Somorjai, J. Y. Park, *Surf. Sci.* **603**, 1293 (2009).
8. J. R. Zheng *et al.*, *Science* **309**, 1338 (2005).
9. J. K. Chung, M. C. Thielges, S. E. J. Bowman, K. L. Bren, M. D. Fayer, *J. Am. Chem. Soc.* **133**, 6681 (2011).
10. Y. S. Kim, R. M. Hochstrasser, *Proc. Natl. Acad. Sci. U.S.A.* **102**, 11185 (2005).
11. D. E. Rosenfeld, Z. Gengeliczki, M. D. Fayer, *J. Phys. Chem. B* **113**, 13300 (2009).
12. D. D. Dlott *et al.*, *J. Am. Chem. Soc.* **118**, 7853 (1996).
13. X. D. Zhu, Y. R. Shen, *Appl. Phys. B* **50**, 535 (1990).
14. Y. Rao, M. Comstock, K. B. Eisenthal, *J. Phys. Chem. B* **110**, 1727 (2006).
15. J. R. Hill *et al.*, *J. Phys. Chem.* **100**, 18023 (1996).
16. I. V. Stiopkin *et al.*, *Nature* **474**, 192 (2011).
17. J. A. McGuire, Y. R. Shen, *Science* **313**, 1945 (2006).
18. E. H. G. Backus, A. Eichler, A. W. Kleyn, M. Bonn, *Science* **310**, 1790 (2005).
19. J. A. Carter, Z. Wang, D. D. Dlott, *Acc. Chem. Res.* **42**, 1343 (2009).
20. A. Eftekhari-Bafrooei, E. Borguet, *J. Phys. Chem. Lett.* **2**, 1353 (2011).
21. I. M. Lane, D. A. King, H. Arnolds, *J. Chem. Phys.* **126**, 024707 (2007).
22. W. Xiong *et al.*, *J. Am. Chem. Soc.* **131**, 18040 (2009).
23. J. Bredenbeck, A. Ghosh, H. K. Nienhuys, M. Bonn, *Acc. Chem. Res.* **42**, 1332 (2009).
24. Y. J. Chabal, P. Dumas, P. Guyot-Sionnest, G. S. Higashi, *Surf. Sci.* **242**, 524 (1991).
25. Z. Gengeliczki, D. E. Rosenfeld, M. D. Fayer, *J. Chem. Phys.* **132**, 244703 (2010).
26. V. Cervetto, J. Helbing, J. Bredenbeck, P. Hamm, *J. Chem. Phys.* **121**, 5935 (2004).
27. N. K. Devaraj, J. P. Collman, *QSAR Comb. Sci.* **26**, 1253 (2007).
28. D. C. Bailey, S. H. Langer, *Chem. Rev.* **81**, 109 (1981).
29. D. E. De Vos, M. Dams, B. F. Sels, P. A. Jacobs, *Chem. Rev.* **102**, 3615 (2002).
30. A. J. Morris, G. J. Meyer, E. Fujita, *Acc. Chem. Res.* **42**, 1983 (2009).
31. H. C. Kolb, M. G. Finn, K. B. Sharpless, *Angew. Chem. Int. Ed.* **40**, 2004 (2001).
32. J. Umemura, T. Kamata, T. Kawai, T. Takenaka, *J. Phys. Chem.* **94**, 62 (1990).
33. Y. Zhang, M. A. Firestone, T. B. Rauchfuss, P. W. Bohn, *J. Phys. Chem.* **100**, 13804 (1996).

34. J. P. Collman, N. K. Devaraj, T. P. A. Eberspacher, C. E. D. Chidsey, *Langmuir* **22**, 2457 (2006).
35. S. Park, K. Kwak, M. D. Fayer, *Laser Phys. Lett.* **4**, 704 (2007).
36. K. Kwak, S. Park, I. J. Finkelstein, M. D. Fayer, *J. Chem. Phys.* **127**, 124503 (2007).
37. K. Kwak, D. E. Rosenfeld, M. D. Fayer, *J. Chem. Phys.* **128**, 204505 (2008).
38. V. M. Kenkre, A. Tokmakoff, M. D. Fayer, *J. Chem. Phys.* **101**, 10618 (1994).
39. R. K. Hocking, T. W. Hambley, *Organometallics* **26**, 2815 (2007).
40. S. Yamamoto, A. Ghosh, H.-K. Nienhuys, M. Bonn, *Phys. Chem. Chem. Phys.* **12**, 12909 (2010).
41. T. Förster, *Radiat. Res. Suppl.* **2**, 326 (1960).
42. D. L. Huber, D. S. Hamilton, B. Barnett, *Phys. Rev. B* **16**, 4642 (1977).
43. R. B. Williams, R. F. Loring, M. D. Fayer, *J. Phys. Chem. B* **105**, 4068 (2001).
44. C. J. Fecko, J. J. Loparo, S. T. Roberts, A. Tokmakoff, *J. Chem. Phys.* **122**, 054506 (2005).

Acknowledgments: The authors thank C. Xie and B. Cui for preparation of the SiO_2-coated CaF_2 substrates and D. B. Wong for making the bulk solution orientational relaxation measurements. D.E.R. acknowledges the support of the Fannie and John Hertz Foundation, a National Science Foundation Graduate Research Fellowship, and a Stanford Graduate Fellowship. This material is based on work supported by the Air Force Office of Scientific Research under AFOSR grant F49620-01-1-0018 and the Department of Energy under grant DE-FG03-84ER13251. In addition, B.J.S. and T.D.P.S. thank the National Institutes of Health (GM50730).

Supporting Online Material

www.sciencemag.org/cgi/content/full/science.1211350/DC1
Materials and Methods
SOM Text
Figs. S1 to S10
Tables S1 and S2
References (*45*–*64*)

18 July 2011; accepted 14 September 2011
Published online 20 October 2011;
10.1126/science.1211350